Development of a Homodyne Detection Tomography Approach

Master Thesis

University of Crete, FORTH IESL

Lamprou Theocharis

Supervisor:Tzallas Paraskevas (Research Director at IESL-FORTH)

Heraklion, Tuesday 10th March, 2020

Abstract

The present work aims to develop a phase sensitive homodyne detection tomography approach that will be used for the characterization of the quantum state of a laser field. The approach will be based on the development of an ultra–stable phase sensitive interferometric arrangement capable to provide measurements of the field quadratures beyond the classical limit.

Contents

Chapter 1

Coherent States of Light, Homodyne Detection

1.1 Introduction

In the present chapter we will briefly describe how the quantization of the Electromagnetic (E/M) field can lead to a possible state which is called "Coherent state of light"[1][2]. We will obtain expressions for the operators that represent the field observables and study their properties as presented in [3][4]. More emphasis is given to the properties of this state of light instead of its explicit derivation. Finally, we will present a well known phase sensitive method, called "Homodyne Detection", by means of which we are able to measure the properties of the signal field we are interested.

1.2 Maxwell's Equations

The E/M field in a non-dispersive, non-absorbing, homogeneous medium can be expressed by the Maxwell's equations:

$$\vec{\nabla} \times \vec{E} = -\frac{\partial \vec{B}}{\partial t} \tag{1.1}$$

$$\vec{\nabla} \times \vec{H} = \frac{\partial \vec{D}}{\partial t} + \vec{J} \tag{1.2}$$

$$\vec{\nabla} \vec{D} = \rho \tag{1.3}$$

$$\vec{\nabla} \vec{B} = 0 \tag{1.4}$$

where ρ, $\vec{J}$ are the charge and current density, respectively. Furthermore, the classical fields are functions of position and time, but here we use a shorter notation $\vec{E} = \vec{E}(\vec{r}, t)$, $\vec{B} = \vec{B}(\vec{r}, t)$. In order to arrive at the quantization of the E/M field, we need to substitute

into the Maxwell's equations the scalar and vector potential,

$$\vec{\nabla}\phi = -\vec{E} - \frac{\partial \vec{A}}{\partial t} \quad and \quad \vec{B} = \vec{\nabla} \times \vec{A} \tag{1.5}$$

after substituting the Eq.1.5 into Eq.1.2,1.3 we obtain the following equations that scalar and vector potential satisfy:

$$\vec{\nabla}(\vec{\nabla}\vec{A}) - \nabla^2\vec{A} + \frac{1}{c^2}\frac{\partial}{\partial t}\nabla\phi + \frac{1}{c^2}\frac{\partial^2\vec{A}}{\partial t^2} = \mu_0\vec{J} \tag{1.6}$$

$$\nabla^2\phi + \frac{\partial}{\partial t}(\vec{\nabla}\vec{A}) = -\frac{\rho}{\epsilon} \tag{1.7}$$

The above equations can be simplified by taking the advantage of *gauge invariance* of the Maxwell's equations, namely, the $\vec{E}$ and $\vec{B}$ are left unchanged under the *gauge transformation*:

$$\begin{aligned} \vec{A} &\longrightarrow \vec{A} = \vec{A}' - \nabla\chi \\ \phi &\longrightarrow \phi = \phi' + \frac{\partial}{\partial t}\chi \end{aligned} \tag{1.8}$$

Assuming that the E/M field is propagating in free space ($\rho, \vec{J} = 0$), choosing the vector and scalar potentials in order that satisfy the conditions $\nabla\vec{A} = 0$ (*Coulomb gauge*) and $\phi = 0$, respectively we end up to the following equation for the vector potential:

$$\nabla^2\vec{A} - \frac{1}{c^2}\frac{\partial^2}{\partial t^2}\vec{A} = 0 \tag{1.9}$$

If we consider a cubic region of space of side L, Fig.1.1,we take running waves and subject them to periodic boundary conditions.

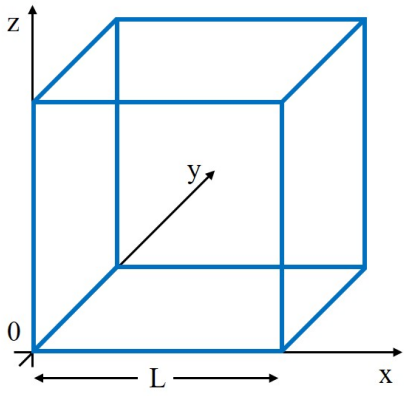

Figure 1.1: Schematic representation of the quantization cavity cube of side L

Therefore, the solution of Eq.1.9, becomes:

$$\vec{A}(\vec{r},t) = \sum_{\vec{k}} \sum_{p=1,2} \hat{e}_{\vec{k},p}\ A_{\vec{k},p}(\vec{r},t) \tag{1.10}$$

where,

$$A_{\vec{k},p}(\vec{r},t) = A_{\vec{k},p} e^{i(\vec{k}\vec{r}-\omega_k t)} + c.c. \tag{1.11}$$

$\omega_k = ck$ is the mode angular frequency and the components of the wavevector $\vec{k}$, take the values:

$$k_i = 2\pi n_i/L, \quad i = x, y, z \ and \ n_i = 0, \pm 1, \pm 2, ... \tag{1.12}$$

Furthermore, $\hat{e}_{\vec{k},p}$ are the unit polarization vectors and the *Coulomb gauge* condition implies that wavevector and polarization vectors are transverse: $\vec{k} \cdot \hat{e}_{\vec{k},p} = 0$. We have chosen the polarizations to be perpendicular with each other: $\hat{e}_{\vec{k},p} \cdot \hat{e}_{\vec{k},p'} = \delta_{p,p'}$.

From Eq.1.5 we get that $\vec{E} = -\frac{\partial \vec{A}}{\partial t}$, since we chose $\phi = 0$. Therefore, the electric field inside the quantization cavity is:

$$\vec{E}(\vec{r},t) = \sum_{\vec{k}} \sum_{p=1,2} \hat{e}_{\vec{k},p}\ E_{\vec{k},p}(\vec{r},t) \tag{1.13}$$

where,

$$E_{\vec{k},p}(\vec{r},t) = i\omega_k A_{\vec{k},p} e^{i(\vec{k}\vec{r}-\omega_k t)} + c.c. \tag{1.14}$$

The magnetic field is also obtained from Eq.1.5:

$$\vec{B}(\vec{r},t) = \sum_{\vec{k}} \sum_{p=1,2} \frac{\vec{k} \times \hat{e}_{\vec{k},p}}{k}\ B_{\vec{k},p}(\vec{r},t) \tag{1.15}$$

where,

$$B_{\vec{k},p}(\vec{r},t) = ikA_{\vec{k},p} e^{i(\vec{k}\vec{r}-\omega_k t)} + c.c. \tag{1.16}$$

Now we are ready to calculate the total energy of the E/M field inside the quantization cavity:

$$\mathcal{H} = \frac{1}{2} \int_{Cavity} dV [\epsilon_0 \vec{E} \cdot \vec{E} + \mu_0^{-1} \vec{B} \cdot \vec{B}] \tag{1.17}$$

By substitution of Eq.1.13 and 1.15 into Eq.1.17 we get:

$$\mathcal{H} = \sum_{\vec{k}} \sum_{p} \mathcal{H}_{\vec{k},p} \tag{1.18}$$

where,

$$\mathcal{H}_{\vec{k},p} = \epsilon_0 V \omega_k^2 (A_{\vec{k},p} A^*_{\vec{k},p} + A^*_{\vec{k},p} A_{\vec{k},p}) \tag{1.19}$$

in the Eq.1.19, we have left the $A_{\vec{k},p}$ and $A^*_{\vec{k},p}$ as they occur in the calculations in order to match this expression with the respective one in the Quantum Harmonic Oscillator.

1.3 Quantum Harmonic Oscillator

The Hamiltonian for a one-dimensional Quantum-Mechanical Harmonic Oscillator (Q/M H.O) is:

$$\hat{\mathcal{H}} = \frac{\hat{p}^2}{2m} + \frac{1}{2} m\omega^2 \hat{q}^2 \tag{1.20}$$

where the position $\hat{q}$ and momentum $\hat{p}$ operators obey the commutation relation:

$$[\hat{q}, \hat{p}] = \hat{q}\hat{p} - \hat{p}\hat{q} = i\hbar \quad \text{or} \quad (\Delta q)(\Delta p) \geq \frac{\hbar}{2} \tag{1.21}$$

It is more convenient to replace the position and momentum operators by a pair of dimensionless operators defined as:

$$\begin{aligned} \hat{a} &= (2m\hbar\omega)^{-1/2}(m\omega\hat{q} + i\hat{p}) \\ \hat{a}^\dagger &= (2m\hbar\omega)^{-1/2}(m\omega\hat{q} - i\hat{p}) \end{aligned} \tag{1.22}$$

The operators $\hat{a}$ and $\hat{a}^\dagger$ are called, respectively, the *annihilation* and *creation* operators for the harmonic oscillator.

From Eq.1.22 it follows that:

$$\begin{aligned} \hat{a}\hat{a}^\dagger &= (2m\hbar\omega)^{-1}(\hat{p}^2 + m^2\omega^2\hat{q}^2 - im\omega\hat{q}\hat{p} + im\omega\hat{p}\hat{q}) \\ &= (2m\hbar\omega)^{-1}(\hat{p}^2 + m^2\omega^2\hat{q}^2 - im\omega[\hat{q}, \hat{p}]) \\ &= (2m\hbar\omega)^{-1}(\hat{p}^2 + m^2\omega^2\hat{q}^2 + m\omega\hbar) \\ &= (\hbar\omega)^{-1}\left(\hat{\mathcal{H}} + \frac{1}{2}\hbar\omega\right) \end{aligned} \tag{1.23}$$

and

$$\hat{a}^\dagger\hat{a} = (\hbar\omega)^{-1}\left(\hat{\mathcal{H}} - \frac{1}{2}\hbar\omega\right) \tag{1.24}$$

The difference and sum of Eq.1.23 and 1.24 provide the expressions for the commutation relation and the Hamiltonian, respectively:

$$[\hat{a}, \hat{a}^\dagger] = \hat{a}\hat{a}^\dagger - \hat{a}^\dagger\hat{a} = 1 \tag{1.25}$$

$$\hat{\mathcal{H}} = \frac{1}{2}\hbar\omega(\hat{a}\hat{a}^\dagger + \hat{a}^\dagger\hat{a}) = \hbar\omega\left(\hat{a}^\dagger\hat{a} + \frac{1}{2}\right) \tag{1.26}$$

Now let us consider $|n\rangle$ be an energy eigenstate (*number states*) of $\hat{\mathcal{H}}$ with eigenvalue E_n.

$$\hat{\mathcal{H}}|n\rangle = E_n|n\rangle \tag{1.27}$$

By properly manipulating the Eq.1.26 we are led to the following expressions and properties for E_n and $|n\rangle$:

$$\begin{aligned} E_n &= \left(n + \frac{1}{2}\right)\hbar\omega, \ \ (n = 0, 1, 2, ...) \\ \hat{a}|n\rangle &= \sqrt{n}|n-1\rangle \\ \hat{a}^\dagger|n\rangle &= \sqrt{n+1}|n+1\rangle \\ \hat{N}|n\rangle &= \hat{a}^\dagger\hat{a}|n\rangle = n|n\rangle \end{aligned} \tag{1.28}$$

where, n denotes the energy levels of the Q/M H.O. In Eq.1.28 is apparent the role of *creation* and *annihilation* operators. They add or subtract a quantum $\hbar\omega$ to or from the total energy, respectively. The ground state of the Q/M H.O is denoted as $|0\rangle$ and since the is no lower state that the ground state, $\hat{a}|0\rangle = 0$.

1.4 Quantization of Electromagnetic Field

In section 1.2 we defined a quantization cavity in order to solve the Eq.1.9, therefore, the quantization of the E/M field is achieved by associating the Q/M H.O with each mode of the radiation in the quantization cavity. A convenient starting point is to introduce the following variables:

$$\begin{aligned} q_{\vec{k},p} &= (\epsilon_0 V)^{1/2}[A_{\vec{k},p} + A^*_{\vec{k},p}] \\ p_{\vec{k},p} &= \frac{1}{i}(\epsilon_0 V\omega_k^2)^{1/2}[A_{\vec{k},p} - A^*_{\vec{k},p}] \end{aligned} \tag{1.29}$$

Now, modifying the eq.1.19 leads us to the following equation for the Hamiltonian of the free electromagnetic field:

$$\mathcal{H} = \frac{1}{2}\sum_{\vec{k}}\sum_{p}[p^2_{\vec{k},p} + \omega_k q^2_{\vec{k},p}] \tag{1.30}$$

Therefore, the Hamiltonian takes the form similar to the harmonic oscillator's, with "mass" equal to unity. Thus, the *annihilation* and *creation* oparators take the form:

$$\begin{aligned} \hat{a}_{\vec{k},p} &= (2\hbar\omega_k)^{-1/2}(\omega_k\hat{q}_{\vec{k},p} + i\hat{p}_{\vec{k},p}) \\ \hat{a}^\dagger_{\vec{k},p} &= (2\hbar\omega_k)^{-1/2}(\omega_k\hat{q}_{\vec{k},p} - i\hat{p}_{\vec{k},p}) \end{aligned} \tag{1.31}$$

with the physical interpretation that the operators respectively destrory and create one

photon of energy $\hbar\omega_k$ in mode $\vec{k}p$. The number of photons excited in a cavity mode is given by the respective operator $\hat{n}_{\vec{k},p}$:

$$\hat{n}_{\vec{k},p}|n_{\vec{k},p}\rangle = \hat{a}^{\dagger}_{\vec{k},p}\hat{a}_{\vec{k},p}|n_{\vec{k},p}\rangle = n_{\vec{k},p}|n_{\vec{k},p}\rangle, \quad n_{\vec{k},p} = 0, 1, 2, ... \tag{1.32}$$

Finally, the Hamiltonian can be written in the following form:

$$\hat{\mathcal{H}} = \sum_{\vec{k}}\sum_{p}\frac{1}{2}\hbar\omega_k\left(\hat{a}_{\vec{k},p}\hat{a}^{\dagger}_{\vec{k},p} + \hat{a}^{\dagger}_{\vec{k},p}\hat{a}_{\vec{k},p}\right) \tag{1.33}$$

This expression allows a direct comparison with Eq.1.19. Therefore, we get the vector potential, electric and magnetic field operators:

$$\hat{\mathbf{A}}(\mathbf{r},t) = \sum_{\mathbf{k}}\sum_{p}\sqrt{\frac{\hbar}{2\epsilon_0 V\omega_k}}\mathbf{e}_{\mathbf{k}p}\left(\hat{a}_{\mathbf{k}p}e^{-i\chi_{\mathbf{k}}(\mathbf{r},t)} - \hat{a}^{\dagger}_{\mathbf{k}p}e^{i\chi_{\mathbf{k}}(\mathbf{r},t)}\right), \tag{1.34a}$$

$$\hat{\mathbf{E}}(\mathbf{r},t) = i\sum_{\mathbf{k}}\sum_{p}\sqrt{\frac{\hbar\omega_k}{2\epsilon_0 V}}\mathbf{e}_{\mathbf{k}p}\left(\hat{a}_{\mathbf{k}p}e^{-i\chi_{\mathbf{k}}(\mathbf{r},t)} - \hat{a}^{\dagger}_{\mathbf{k}p}e^{i\chi_{\mathbf{k}}(\mathbf{r},t)}\right), \tag{1.34b}$$

$$\hat{\mathbf{B}}(\mathbf{r},t) = i\sum_{\mathbf{k}}\sum_{p}\mathbf{k}\times\mathbf{e}_{\mathbf{k}p}\sqrt{\frac{\hbar}{2\epsilon_0 V\omega_k}}\left(\hat{a}_{\mathbf{k}p}e^{-i\chi_{\mathbf{k}}(\mathbf{r},t)} - \hat{a}^{\dagger}_{\mathbf{k}p}e^{i\chi_{\mathbf{k}}(\mathbf{r},t)}\right), \tag{1.34c}$$

where phase $\chi_{\mathbf{k}}$ is defined as: $\chi_{\mathbf{k}}(\mathbf{r},t) = \omega_k t - \mathbf{kr}$.

1.4.1 Coherent States

The *Coherent states* of light, $|\alpha\rangle$, are a linear superposition of *number states* and eigenstates of the annihilation operator $\hat{a}$. They play an important role to quantum optics, not only because their properties are closer to these of classical E/M field but also because coherent states can be produced by a LASER. Since the annihilation operator is a non-Hermitian operator, its eigenvalues can be complex. Therefore, the eigenvalue equation for coherent states is the following:

$$\hat{a}|\alpha\rangle = \alpha|\alpha\rangle, \quad |\alpha\rangle = \sum_{n=0}^{\infty}\langle n|\alpha\rangle|n\rangle \tag{1.35}$$

We wish to find the expression of coherent states as a linear superposition of the number states. So, from Eq.1.35 by multiplication from the left with $\langle n|$ we get:

$$\langle n|\hat{a}|\alpha\rangle = \langle n|\alpha|\alpha\rangle = \alpha\langle n|\alpha\rangle \Rightarrow \left(\langle\alpha|\hat{a}^{\dagger}|n\rangle\right)^{*} = \alpha\langle n|\alpha\rangle \Rightarrow$$

$$\langle n+1|\alpha\rangle = \frac{\alpha}{\sqrt{n+1}}\langle n|\alpha\rangle, \quad n = 0, 1, 2...$$

Now lets apply the above equation for $n = 0$ and $n = 1$ in order to find out the pattern that it follows

$$
\begin{aligned}
n = 0: \quad & \langle 1|\alpha\rangle = \frac{\alpha}{\sqrt{1}}\langle 0|\alpha\rangle \\
n = 1: \quad & \langle 2|\alpha\rangle = \frac{\alpha}{\sqrt{2}}\langle 1|\alpha\rangle = \frac{\alpha^2}{\sqrt{2!}}\langle 0|\alpha\rangle \\
& . \\
& . \\
& . \\
\Rightarrow & \langle n|\alpha\rangle = \frac{\alpha^n}{\sqrt{n!}}\langle 0|\alpha\rangle
\end{aligned}
$$

Therefore Eq.1.35 becomes:

$$
|\alpha\rangle = \sum_{n=0}^{\infty} \frac{\alpha^n}{\sqrt{n!}}\langle 0|\alpha\rangle|n\rangle = \langle 0|\alpha\rangle \sum_{n=0}^{\infty} \frac{\alpha^n}{\sqrt{n!}}|n\rangle \Rightarrow
$$

$$
\langle \alpha|\alpha\rangle = |\langle 0|\alpha\rangle|^2 \sum_{n=0}^{\infty} \frac{|\alpha|^{2n}}{n!} = |\langle 0|\alpha\rangle|^2 \; e^{|\alpha|^2} = 1 \Rightarrow \langle 0|\alpha\rangle = e^{i\phi - \frac{1}{2}|\alpha|^2}
$$

where ϕ is a phase same for all number states so, it plays no role to the total eigenfunction, it can be omitted then. The coherent state in the number states base is written as:

$$
|\alpha\rangle = e^{-\frac{1}{2}|\alpha|^2} \sum_{n=0}^{\infty} \frac{\alpha^n}{\sqrt{n!}}|n\rangle = e^{-\frac{1}{2}|\alpha|^2} \sum_{n=0}^{\infty} \frac{(\alpha\hat{a}^\dagger)^n}{n!}|0\rangle = e^{\alpha\hat{a}^\dagger - \frac{1}{2}|\alpha|^2}|0\rangle \tag{1.36}
$$

Although number states are orthogonal to each other, coherent states are not orthogonal. Consider two different coherent states $|\alpha\rangle$ and $|\beta\rangle$,

$$
\begin{aligned}
\langle \beta|\alpha\rangle &= e^{-\frac{1}{2}|\alpha|^2} e^{-\frac{1}{2}|\beta|^2} \sum_n \sum_m \frac{\alpha^n}{\sqrt{n!}} \frac{\beta^{*m}}{\sqrt{m!}} \langle m|n\rangle = e^{-\frac{1}{2}(|\alpha|^2+|\beta|^2)} \sum_n \frac{(\alpha\beta^*)^n}{n!} \\
&= e^{\alpha\beta^* - \frac{1}{2}(|\alpha|^2+|\beta|^2)} \neq \delta(\alpha - \beta) \\
&\Rightarrow |\langle \alpha|\beta\rangle|^2 = e^{-|\alpha-\beta|^2}
\end{aligned} \tag{1.37}
$$

Based on the *Baker-Campell-Haussdorf* relation,

$$
e^{(\hat{A}+\hat{B})} = e^{\hat{A}} e^{\hat{B}} e^{-\frac{1}{2}[\hat{A},\hat{B}]}, \quad \text{valid if}: \; [\hat{A},[\hat{A},\hat{B}]] = [\hat{B},[\hat{A},\hat{B}]] = 0 \tag{1.38}
$$

Furthermore, $e^{-\alpha^*\hat{a}}|0\rangle = |0\rangle$ and $[\alpha\hat{a}^\dagger, -\alpha^*\hat{a}] = |\alpha|^2$. Thus from Eq.1.36 and 1.38,

$$
|\alpha\rangle = e^{\alpha\hat{a}^\dagger - \frac{1}{2}|\alpha|^2}|0\rangle = e^{\alpha\hat{a}^\dagger - \frac{1}{2}|\alpha|^2} e^{-\alpha^*\hat{a}}|0\rangle = e^{(\alpha\hat{a}^\dagger - \alpha^*\hat{a})}|0\rangle \tag{1.39}
$$

This result is written as:

$$
|\alpha\rangle = \hat{D}(\alpha)|0\rangle \tag{1.40}
$$

where $\hat{D}(\alpha) = e^{(\alpha\hat{a}^\dagger - \alpha^*\hat{a})}$ is the *coherent-state displacement operator*, which is also a unitary operator, since $\hat{D}(\alpha)\hat{D}^\dagger(\alpha) = \hat{D}^\dagger(\alpha)\hat{D}(\alpha) = 1$. Its effect on the annihilation and creation will also be useful:

$$\begin{aligned} \hat{D}^\dagger(\alpha)\hat{a}\hat{D}(\alpha) &= \hat{a} + \alpha \\ \hat{D}^\dagger(\alpha)\hat{a}^\dagger\hat{D}(\alpha) &= \hat{a}^\dagger + \alpha^* \end{aligned} \tag{1.41}$$

We now consider the time evolution of a single-mode coherent state, by acting with the time evolution operator $\hat{\mathcal{U}}(t) = e^{-i\hat{\mathcal{H}}t/\hbar}$, to the time independent coherent state $|\alpha\rangle$.

$$\begin{aligned} |\alpha, t\rangle &= \hat{\mathcal{U}}(t)|\alpha\rangle = e^{-i\hat{\mathcal{H}}t/\hbar}|\alpha\rangle = e^{-i\omega t/2}e^{-i\omega t\hat{n}}|\alpha\rangle = e^{-i\omega t/2}e^{-i\omega t\hat{n}}e^{-\frac{1}{2}|\alpha|^2}\sum_{n=0}^{\infty}\frac{\alpha^n}{\sqrt{n!}}|n\rangle \\ &= e^{-i\omega t/2}e^{-\frac{1}{2}|\alpha|^2}\sum_{n=0}^{\infty}e^{-i\omega t\hat{n}}\frac{\alpha^n}{\sqrt{n!}}|n\rangle = e^{-i\omega t/2}e^{-\frac{1}{2}|\alpha|^2}\sum_{n=0}^{\infty}e^{-i\omega tn}\frac{\alpha^n}{\sqrt{n!}}|n\rangle \\ &= e^{-i\omega t/2}e^{-\frac{1}{2}|\alpha|^2}\sum_{n=0}^{\infty}\frac{(e^{-i\omega t}\alpha)^n}{\sqrt{n!}}|n\rangle = e^{-i\omega t/2}|\alpha e^{-i\omega t}\rangle \end{aligned} \tag{1.42}$$

The last property which is important to punctuate is the uncertainty relation between the position and momentum operators.

$$\hat{q} = \left(\frac{\hbar}{2\omega}\right)^{1/2}(\hat{a}^\dagger + \hat{a}) \quad \text{and} \quad \hat{p} = i\left(\frac{\hbar\omega}{2}\right)^{1/2}(\hat{a}^\dagger - \hat{a}) \tag{1.43}$$

By taking the expectation value of these operators for a coherent state, we get:

$$\langle\hat{q}\rangle_\alpha = \langle\alpha|\hat{q}|\alpha\rangle = 2\left(\frac{\hbar}{2\omega}\right)^{1/2}|\alpha|cos(\theta) \tag{1.44}$$

and

$$\langle\hat{q}^2\rangle_\alpha = \langle\alpha|\hat{q}^2|\alpha\rangle = \frac{\hbar}{2\omega}\left(4|\alpha|^2cos^2(\theta) + 1\right) \tag{1.45}$$

Therefore, the position operator uncertainty is:

$$(\Delta q)^2_\alpha = \langle\hat{q}^2\rangle_\alpha - \langle\hat{q}\rangle_\alpha = \frac{\hbar}{2\omega} \tag{1.46}$$

Similarly, we find the variance of the momentum operator:

$$(\Delta p)^2_\alpha = \langle\hat{p}^2\rangle_\alpha - \langle\hat{p}\rangle_\alpha = \frac{\hbar\omega}{2} \tag{1.47}$$

Using the above results, we calculate the uncertainty relation:

$$(\Delta q)_\alpha(\Delta p)_\alpha = \frac{\hbar}{2} \tag{1.48}$$

Thus, we came to the result that coherent states are **minimum-uncertainty states** because the equation 1.21 is satisfied with equality. In a following section we will see a graphical representation of this result.

1.4.2 Photon Statistics of Coherent States

The coherent-state expectation value for the number operator is obtained with use of the properties 1.41:

$$\langle n\rangle = \langle\alpha|\hat{n}|\alpha\rangle = \langle\alpha|\hat{a}^\dagger\hat{a}|\alpha\rangle = \langle 0|\hat{D}^\dagger(\alpha)\hat{a}^\dagger\hat{D}(\alpha)\hat{D}^\dagger(\alpha)\hat{a}\hat{D}(\alpha)|0\rangle = |\alpha|^2 \tag{1.49}$$

where we also took the advantage that the coherent-state displacement operator is a unitary operator. Following similar steps, we also calculate the photon-number variance:

$$(\Delta n)^2 = \langle n^2\rangle - \langle n\rangle^2 = |\alpha|^2 = \langle n\rangle \tag{1.50}$$

with fractional uncertainty,

$$\frac{\Delta n}{\langle n\rangle} = \frac{1}{\sqrt{\langle n\rangle}} \tag{1.51}$$

which states that the fractional uncertainty goes to zero with increasing the average photon-number, i.e. the intensity.

The probability of finding n photons in the single-mode coherent state is obtained from Eq.1.36:

$$P(n) = |\langle n|\alpha\rangle|^2 = e^{-|\alpha|^2}\left|\langle n|\sum_m \frac{\alpha^m}{\sqrt{m!}}|m\rangle\right|^2 = e^{-|\alpha|^2}\frac{|\alpha|^{2n}}{n!} = e^{-\langle n\rangle}\frac{\langle n\rangle^n}{n!} \tag{1.52}$$

It is obvious from the equation above that photons in the coherent state obey the Poissonian probability distribution. Note also that Poisson distribution approaches a Gaussian distribution for large $\langle n\rangle$.

$$P(n) \approx \frac{1}{\sqrt{2\pi\langle n\rangle}} e^{-\frac{(n-\langle n\rangle)^2}{2\langle n\rangle}} \tag{1.53}$$

1.4.3 Single - mode Electric field operator

The scalar electric field operator of a linearly polarized single-mode, propagating in the z axis is written as:

$$\hat{E}(\chi) = i\sqrt{\frac{\hbar\omega}{2\epsilon_0 V}}\left(\hat{a}e^{-i\chi} - \hat{a}^\dagger e^{i\chi}\right) = \frac{E_0}{2}\left(\hat{a}e^{-i(\chi+\pi/2)} + \hat{a}^\dagger e^{i(\chi+\pi/2)}\right) \tag{1.54}$$

where $E_0 = \sqrt{\frac{2\hbar\omega}{\epsilon_0 V}}$ and $\chi = \omega t - kz$.

The expectation value of the electric field operator is:

$$\langle \hat{E} \rangle = \langle \alpha | \hat{E} | \alpha \rangle = E_0 |\alpha| sin(\chi - \theta) \tag{1.55}$$

which describes the classically oscillating electric field (corresponding figure). We have used again the substitution $\alpha = |\alpha| e^{i\theta}$ for the eigenvalue of the annihilation operator. The expectation value for the E^2 operator is:

$$\langle \hat{E}^2 \rangle = \langle \alpha | \hat{E}^2 | \alpha \rangle = \left(\frac{E_0}{2} \right)^2 (4|\alpha|^2 sin^2(\chi - \theta) + 1) \tag{1.56}$$

Therefore, the uncertainty of the electric field operator is given by:

$$(\Delta E)^2 = \langle \hat{E}^2 \rangle - \langle \hat{E} \rangle^2 = (E_0/2)^2 \tag{1.57}$$

Note that the uncertainty of the field (*noise*) is independent of the photon number of the coherent state. Thus, for very large photon number ($|\alpha|^2$), the uncertainty becomes negligible and the field will tend to its classical representation. On the other hand, for the vacuum state ($|\alpha| = 0$) the mean value is equal to zero, as expected, but there is a non zero uncertainty due to vacuum fluctuations.

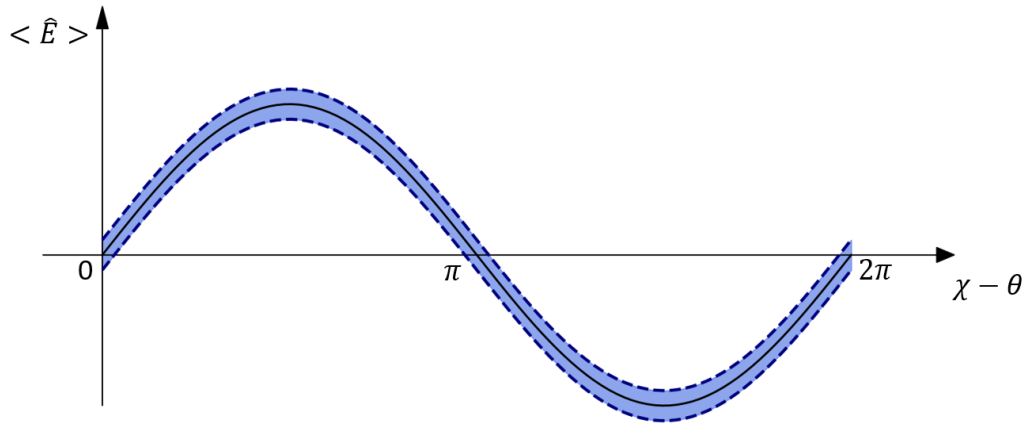

Figure 1.2: Phase dependence of the mean value of the electric field for a coherent state. The black solid line represents the $\langle \hat{E} \rangle$, while the blue shaded area represents the uncertainty of the electric field.

Another useful way to describe an oscillating field is through the phase space, where each point in the phase space corresponds to a unique state of the system. We introduce a new set of dimensionless operators, which are called *quadrature operators*, as:

$$\hat{X} = \frac{\hat{a} + \hat{a}^\dagger}{2} \quad \text{and} \quad \hat{Y} = i\frac{\hat{a}^\dagger - \hat{a}}{2} \tag{1.58}$$

Note that the operators $\hat{X}, \hat{Y}$ are proportional to the position $(\hat{q})$ and momentum $(\hat{p})$ operators, respectively. Now, the electric field operator can be expressed in terms of this new set of operators:

$$\hat{E} = E_0 \left(\hat{X} sin(\chi) - \hat{Y} cos(\chi) \right) \tag{1.59}$$

The mean values and variances of these operators are:

$$\langle \hat{X} \rangle = \langle \alpha | \hat{X} | \alpha \rangle = |\alpha| cos(\theta) \quad \text{and} \quad \langle \hat{Y} \rangle = \langle \alpha | \hat{Y} | \alpha \rangle = |\alpha| sin(\theta) \tag{1.60}$$

and

$$(\Delta X)^2 = \langle \hat{X}^2 \rangle - \langle \hat{X} \rangle^2 = 1/4 \quad \text{and} \quad (\Delta Y)^2 = \langle \hat{Y}^2 \rangle - \langle \hat{Y} \rangle^2 = 1/4 \tag{1.61}$$

Therefore, the minimum uncertainty relation for the operators $\hat{X}$ and $\hat{Y}$ becomes:

$$(\Delta X)(\Delta Y) = 1/4 \tag{1.62}$$

The representation of coherent state in phase space of the two quadrature operators is depicted in the following figure. In the appendix is justified that a coherent state can be expressed as a superposition of eigenstates of either the two quadrature operators, where both superpositions follow the Gaussian probability distribution.

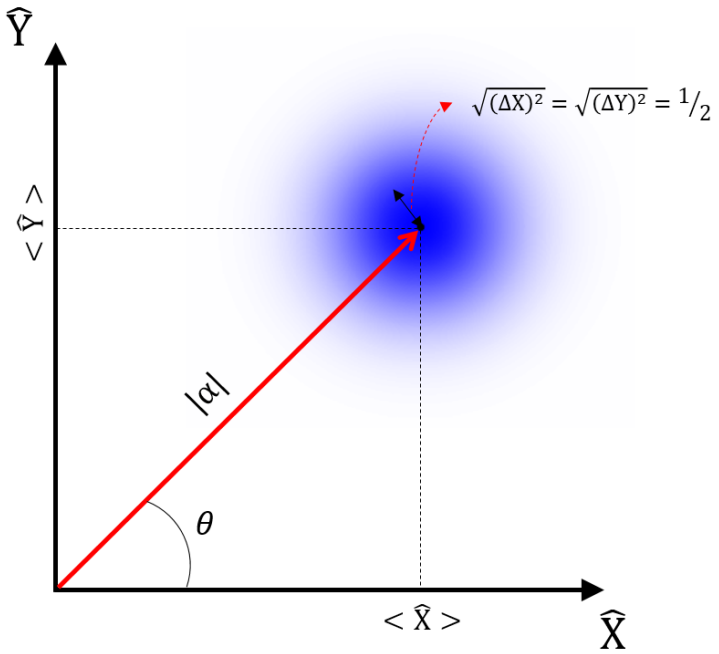

Figure 1.3: Phase space representation of a coherent state $|\alpha\rangle$ with $\alpha = |\alpha| e^{i\theta}$.

Sometimes it is quite useful to write the electric field operator in terms of a generalized quadrature operator defined as:

$$\hat{x}_\Phi = \frac{1}{2}\left(\hat{a}e^{-i\Phi} + \hat{a}^\dagger e^{i\Phi}\right) \tag{1.63}$$

with mean value and uncertainty:

$$\langle \hat{x}_\Phi \rangle = |\alpha| cos(\Phi - \theta) = |\alpha| sin(\chi - \theta) \quad \text{and} \quad (\Delta x_\Phi)^2 = 1/4 \tag{1.64}$$

Therefore the electric field operator becomes:

$$\hat{E} = E_0 \hat{x}_\Phi \tag{1.65}$$

where in this case $\Phi = \chi - \pi/2$. Note that $\hat{x}_0 = \hat{X}$ and $\hat{x}_{\pi/2} = \hat{Y}$.

In the following section we will talk about an experimental setup where it is possible to measure the electric field's quadrature operator and obtain information about the quantum state of the light we are interested in.

1.5 Balanced Homodyne Detection

Homodyne detection measures the electric field quadrature $\hat{x}_\Phi$ of the incident light field as a function of the measurement phase angle[5][6]. The figure below, shows the experimental arrangement for a homodyne detection measurement.

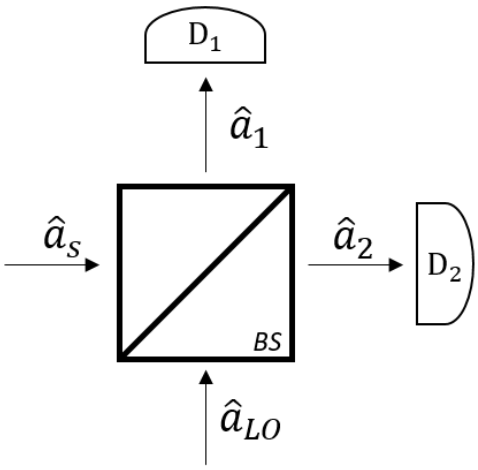

Figure 1.4: Experimental arrangement of optical components in homodyne detection.

As we see in figure 1.4, the signal to be measured ($\hat{a}_s$) interferes with a strong coherent field ($\hat{a}_{LO}$), called *Local Oscillator*, at a beam splitter and the output signals ($\hat{a}_1$, $\hat{a}_2$) are measured at the corresponding detectors. The beam splitter is assumed to be 50:50 with reflection and transmission coefficients given by:

$$R = |R|e^{i\phi_R} = \frac{1}{\sqrt{2}}e^{i\phi_R}, \quad T = |T|e^{i\phi_T} = \frac{1}{\sqrt{2}}e^{i\phi_T}$$
$$\text{and} \quad \phi_R - \phi_T = \pi/2 \tag{1.66}$$

Each detector measures photocounts, namely the number of photons arriving at them. However, we are interested to measure the difference between the number of photons arriving at the two detectors. From the input-output relations for a beam splitter we get:

$$\begin{aligned} \hat{a}_1 &= \frac{1}{\sqrt{2}}(\hat{a}_{LO} + i\ \hat{a}_s) \\ \hat{a}_2 &= \frac{1}{\sqrt{2}}(\hat{a}_s + i\ \hat{a}_{LO}) \end{aligned} \tag{1.67}$$

Using the above equations, we define the homodyne photocurrent operator as:

$$\begin{aligned} \hat{N} &= \hat{a}_2^\dagger \hat{a}_2 - \hat{a}_1^\dagger \hat{a}_1 \\ &= i\left[\hat{a}_s^\dagger \hat{a}_{LO} - \hat{a}_{LO}^\dagger \hat{a}_s\right] \end{aligned} \tag{1.68}$$

The phase difference between the *signal* and the LO can be changed externally by varying the length of the LO optical path. This means that the LO mode operators are subjected to the following phase shift:

$$\begin{aligned} \hat{a}_{LO} &\to \hat{a}_{LO} e^{i\phi_D} \\ \hat{a}_{LO}^\dagger &\to \hat{a}_{LO}^\dagger e^{-i\phi_D} \end{aligned} \tag{1.69}$$

Thus, the homodyne photocurrent operator becomes:

$$\hat{N} = i\left[\hat{a}_s^\dagger \hat{a}_{LO} e^{i\phi_D} - \hat{a}_{LO}^\dagger e^{-i\phi_D} \hat{a}_s\right] \tag{1.70}$$

The expectation value of the homodyne photocurrent operator is:

$$\begin{aligned} \langle \hat{N} \rangle &= \langle \alpha_s, \alpha_{LO} | \hat{N} | \alpha_s, \alpha_{LO} \rangle \\ &= |\alpha_{LO}| \langle \alpha_s | \left(\hat{a}_s e^{-i\Phi} + \hat{a}_s^\dagger e^{i\Phi} \right) | \alpha_s \rangle \\ &= 2|\alpha_{LO}| \langle \hat{x}_\Phi \rangle_s \end{aligned} \tag{1.71}$$

In a similar way we calculate the uncertainty:

$$\begin{aligned} (\Delta N)^2 &= \langle \hat{N}^2 \rangle - \langle \hat{N} \rangle^2 \\ &= 4|\alpha_{LO}|^2 \langle \hat{x}_\Phi^2 \rangle_s + \langle \hat{a}_s^\dagger \hat{a}_s \rangle - 4|\alpha_{LO}|^2 \langle \hat{x}_\Phi \rangle_s^2 \\ &= 4|\alpha_{LO}|^2 (\Delta x_\Phi)_s^2 + \langle \hat{a}_s^\dagger \hat{a}_s \rangle \\ &= 4|\alpha_{LO}|^2 \left[(\Delta x_\Phi)_s^2 + \frac{\langle \hat{a}_s^\dagger \hat{a}_s \rangle}{4|\alpha_{LO}|^2} \right] \end{aligned} \tag{1.72}$$

We should note, here, that the phase Φ contains the phase difference induced, the $\pi/2$ phase from the eq.1.68 and has also absorbed the argument of α_{LO}. We came into a result that balanced homodyne detection measures the quadrature of the signal field including a scaling factor $2|\alpha_{LO}|$.

In the right hand of eq.1.72 there are two terms inside the brackets. The first one is the uncertainty of the **signal field's** *generalized operator*, $\hat{x}_\Phi$, while the second one is the ratio between the mean photon number of the signal pulse $(\langle \hat{a}_s^\dagger \hat{a}_s \rangle) = |\alpha_s|^2$ and the mean photon number of the *LO* pulse ($|\alpha_{LO}|^2$). Our aim is to measure the qudrature of the signal field, therefore, if the intensity of the *Local Oscillator* (i.e. the *LO*'s mean photon number) is much stronger than the signal field's intensity, the second term of the eq.1.72 becomes negligible compared with the first one which is equal to 1/4. So, for $|\alpha_{LO}|^2 >> |\alpha_s|^2$:

$$(\Delta N)^2 \cong 4|\alpha_{LO}|^2 \ (\Delta x_\Phi)_s^2 \tag{1.73}$$

We have almost reached the wanted result, since in both equations 1.71 and 1.73, there is a scaling factor. Therefore, by redefining the *homodyne photocurrent operator*, $\hat{N}$, as $\hat{N}' = \hat{N}/(2|\alpha_{LO}|)$ we conclude:

$$\langle \hat{N}' \rangle = \langle \hat{x}_\Phi \rangle_s \ \ and \ \ (\Delta N')^2 = (\Delta x_\Phi)_s^2 \tag{1.74}$$

Comparing the result above with the equations 1.55, 1.57, the fulfillment of the contition $|\alpha_{LO}| >> |\alpha_s|$, i.e. the intensity of the LO is much greater than the intensity of the signal we want to measure, makes possible to a balanced homodyne detection experimental setup to characterize the quantum state of light.

Chapter 2

Experiment

2.1 Introduction

In this chapter we are going to describe the experimental setup used for the measurement of the coherent state of a laser field. Then, we will present the measurements performed about the stability characterization of the interferometer and consequently the calculations regarding the coherent state of LASER.

2.2 Experimental Setup

In the following figure 2.1, we present the experimental setup we used for the homodyne measurements.

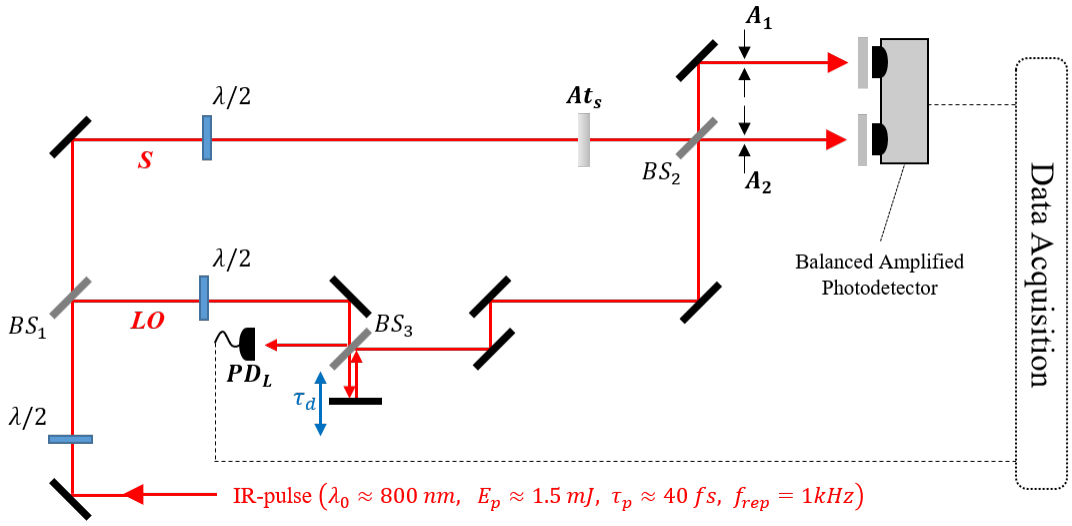

Figure 2.1: Schematic representation of the experimental setup used for the homodyne measurement

A $\approx$ 40 fs Ti:Sapphire linearly polarized laser pulse of 800 nm carrier wavelength, 1kHz repetition rate and $\approx$ 0.6 mJ energy per pulse is entering the Mach - Zehnder interfomenter in BS_1 and split by two. In both arms there are $\lambda/2$ plates to control the

polarization in order that the BS_2 act as 50:50 for each beam. The two $\lambda/2$ plates are rotated at the same angle because the interference term when two beams come together is proportional to the dot product of their polarization vectors. The reflected beam corresponds to the *Local Oscillator*, which is also divided in the BS_3 in order to: a) record the pulse energy (Laser stability) using the photodiode PD_L and b) introduce delay using a mirror placed on a piezoelectric stage, as it is shown in figure 2.1. Finally, the LO pulse arrives at the BS_2 where it interferes with the *Signal* pulse and exits the interferometer. On the other hand, the transmitted part of the beam incident on BS_1 is considered as the *Signal Field* and passes through a variable attenuator before reaching the BS_2 and interferes with LO. At the exit arms of the Mach - Zehnder interferometer there are two apertures through which only ($\varnothing 1.9\ mm$) the central part of the beam is allowed to pass. In this way, we increase the contrast of the interferences resulted by the superposition of the *Signal* and LO fields. Finally, the two signals are incident on a balanced amplified photodetector in front of which there are OD filters in order to avoid the saturation of its photodiodes. The output of the photodetector is the subtraction of the two signals and is recorded by our data acquisition system.

2.3 Photodetector Linearity

The first characterization of the balanced amplified photodetector is to test the linearity of each photodiode independently. In order to do that, we keep one photodiode open each time and we measure the output signal as a function of the LO power. The signal was recorded on the oscilloscope with average of 10 pulses.

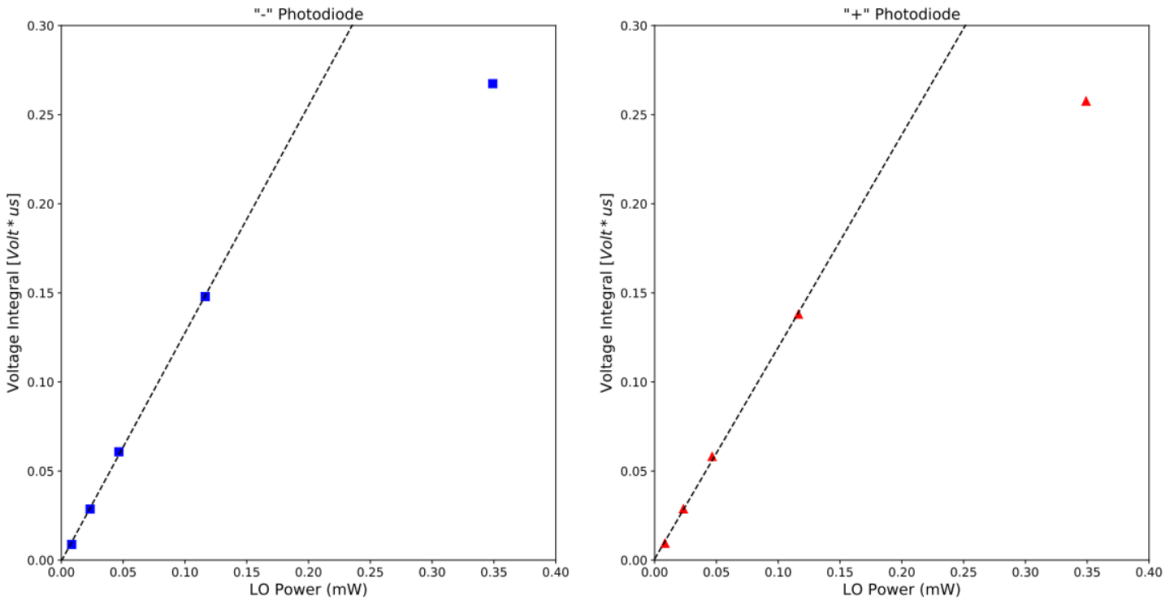

Figure 2.2: Linearity test measurements of the balanced amplified photodetector photodiodes. The left graph is referred to the "minus" photodiode (the one whose signal is inverted) and the right graph to the "plus" photodiode.

The measurements are presented in figure 2.2 where a linear fit is also shown. We note that the response of the photodiodes is linear up to $\sim 0.12\ mW$ LO power, therefore, we take care to keep the LO power below that value.

2.4 Detector Stability

The stability of the detector is crucial for long term accurate measurements. The imbalance of the detector leads to a shift of the detector baseline which is usually linear over time and thus cause detection errors. Therefore, it is important to evaluate the stability of our detection system. A method to obtain quantitative information about possible detector imbalances is through the *Allan Variance*[7]. In the following subsection, we will explain with a simple examples what is the *Allan Variance* calculation. In the subsection 2.4.2 we will present our measurements and how the information that *Allan Variance* gives us is treated.

2.4.1 Allan Variance

Description of Allan Variance

In the following figure we see a time signal with sample rate $1/\tau_0$. What *Allan Variance*[8] algorithm actually does is that it makes temporal windows which are integer multiples of τ_0 and starts scanning the signal as it is depicted in figure 2.3.

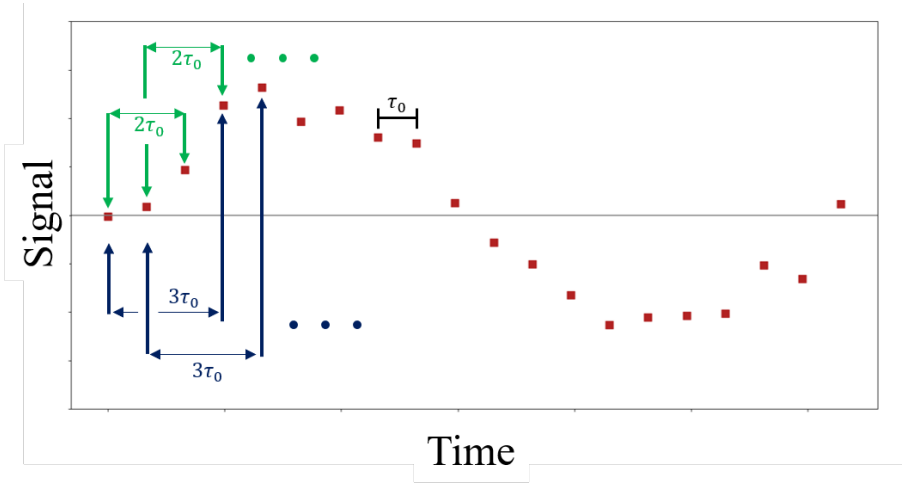

Figure 2.3: Time signal with sample rate $1/\tau_0$. It also depicts how the *Allan Variance* algorithm is working for two different time intervals ($2\tau_0$ and $3\tau_0$).

So, for each temporal window $m\tau_0$, we obtain a list of variances given from the following formula called *Overlapped Allan Variance*:

$$\sigma^2(m\tau_0) = \frac{1}{2m^2(N-2m+1)} \sum_{j=1}^{N-2m+1} \sum_{i=j}^{j+m-1} (y_{i+m} - y_i)^2 \tag{2.1}$$

where, N is the number of samples and the integer $m \leq \frac{N-1}{2}$ and $y_i = \frac{x_{i+1}-x_i}{\tau_0}$ is the fractional frequency.

In figure 2.4a we present a signal which follows a Gaussian distribution with standard deviation $\sigma = 0.1$ $[S]$. In this signal we have added a baseline which increases linearly over time. What we observe is that at low values of τ the Allan variance is high due to high noise. As the τ increases, the Allan Variance drops because the noise averages out. For higher τ's the baseline inclination starts playing important role, so the variance

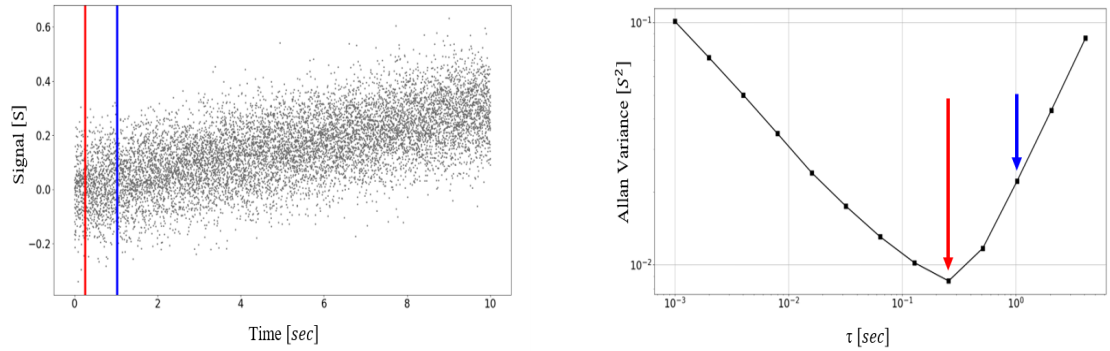

(a) Time Signal

(b) Allan Variance

Figure 2.4: a) Example of a signal where the detector's baseline changes linearly over time and b) the respective Overlapped Allan Variance calculation

increases again. Therefore, we trace the τ_{min} for which the Allan Variance takes its minimum value (red line and arrow in figure 2.4b) and we recalibrate our signal every $t = \tau_{min}$ in order to fix the offset.

2.4.2 Detector Stability measurements

In order to check the stability of our detector, we have blocked the signal arm and recorded the homodyne signal of vacuum state for about 4 minutes ($240[sec] \times 500\left[\frac{points}{sec}\right] = 120000$ *total points*). After that we performed the Allan Variance calculation in order to find out if the baseline of our detector remains constant. In the figures below, we present the measured data and the Allan Variance graph.

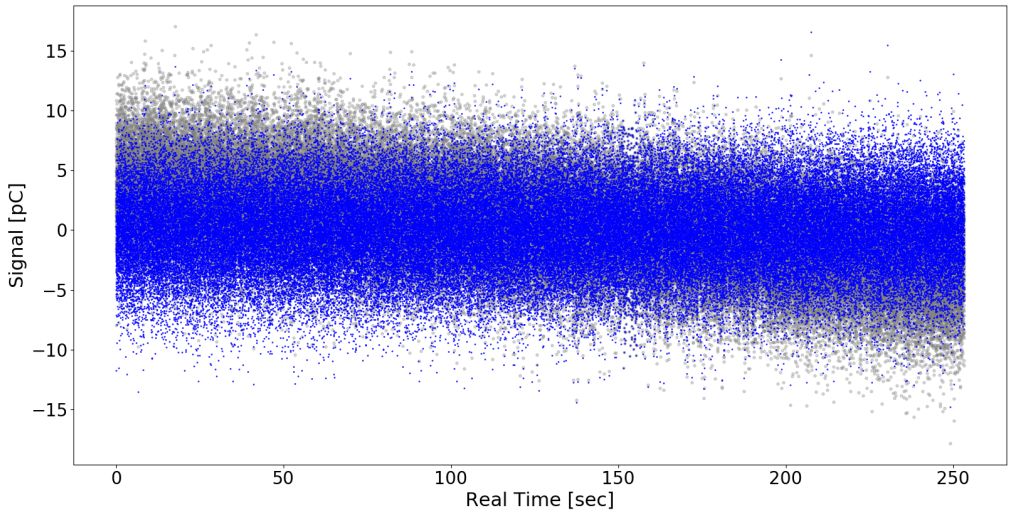

Figure 2.5: Vacuum state homodyne signal. The gray data points represent the raw data. The baseline shift is obvious. The blue data points resulted from recalibration of the raw data.

In figure 2.5 we see the recorded data of the vacuum input state (gray points). It is obvious that the detector's baseline has a linear shift over time. Performing the *Overlapped Allan Variance* calculation one gets the graph 2.6a. As we expected, in the *Allan Variance* plot appears a minimum at τ_{min} and for higher values of τ the baseline shift leads to the increment of *Allan Variance*. Therefore, we construct bins of temporal length equal to τ_{min} and we recalibrate the vacuum state signal. The *Allan Variance* of the recalibrated signal 2.6b has a continuous reduction since the baseline shift has been removed.

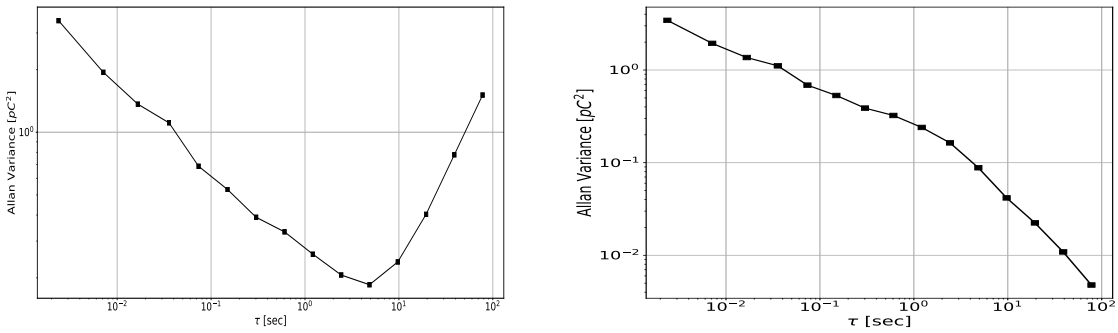

(a) Raw data (b) Recalibrated data

Figure 2.6: *Overlapped Allan Variance* calculation of the a) raw data of vacuum state input field (gray data points of fig.2.5) and b) recalibrated data (blue data points of fig.2.5)

2.5 Shot Noise

There is another test to study the performance of our detector is to measure the response of shot noise as we increase the LO power. The shot noise results from the fact that the pulses of the laser are not completely identical. In the figure below 2.7

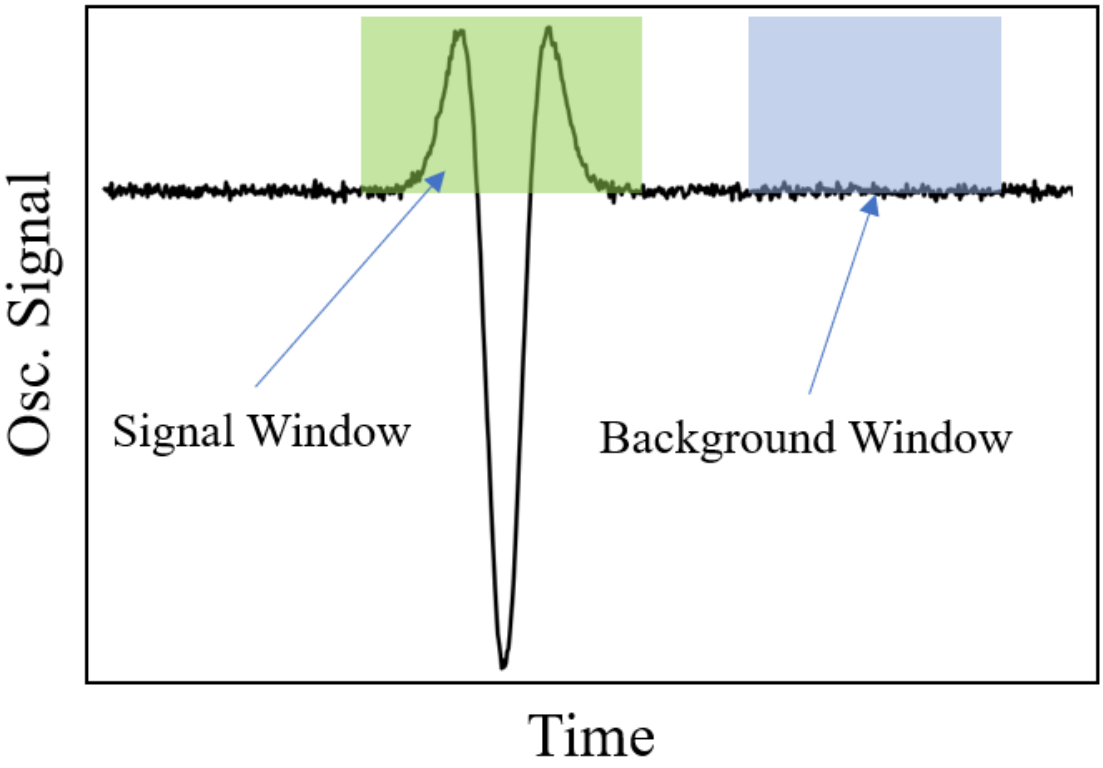

Figure 2.7: The detector's output signal as it appears on the oscilloscope's screen

we show how the signal of the detector appears on the oscilloscope. The shot noise linearity test include time traces like that of figure 2.5 for the *Homodyne* signal and the respective background. We record the signal in both windows (*Detector output signal* and *Background*) at the same time and we calculate the noise in each temporal window. The detector's output signal noise is composed from two individual noise sources. The first one is the *electronic* noise, which is calculated from the *background* window, and the second one is the *shot* noise. These two noise sources are completely uncorrelated to each other, therefore, we can calculate the shot noise by subtracting the electronic noise from the detector output signal noise. What we expect from eq.1.72 is that the homodyne shot noise will change linearly with respect to LO power since the uncertainty of the homodyne photocurrent operator is proportional to the LO mean photon number. The measurements are presented below in a Log−Log graph.

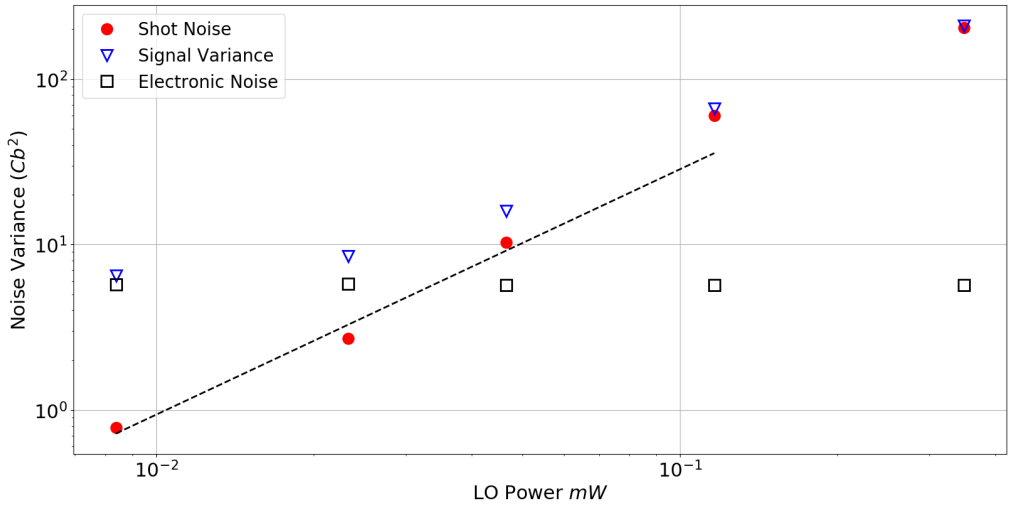

Figure 2.8: Log−Log plot of the shot noise measurements.

The LO powers used are similar to those used for the figure 2.2. We performed the *overlapped Allan Variance* calculation for each time trace and recalibrated the signal if needed. In order to calculate the *shot noise*, we subtract the *electronic noise* from the *signal noise* (since they are non−correlated signals). As we explained earlier, we expect a linear dependence of the shot with respect to the LO power. In order to calculate the slope, we used the first three points and the result is $\approx 1.3 \pm 0.2$. This slope value is acceptable, considering the error of the calculation, however we choose to work at around 0.03 mW LO power in order to be sure.

2.6 Homodyne Measurements

After the detector characterization, the homodyne measurements followed for different *signal* input power. First of all, we need to find the correct position for the piezo where the pulses of the two arms actually interfere. This piezo is attached on a translation stage which can be moved with a picomotor. We ended up with this setup because our piezo cannot perform scans greater than $\sim 2.5\ \mu m$ ($\sim$6 cycles of IR). Therefore, we run a first order autocorrelation scan with the picomotor stage, a part of which is shown in the figure below 2.9, with steps of $\sim 40\ nm$. In this scan, the variable attenuator in the signal arm was rotated so that the signal was attenuated by a factor of ~ 100 (OD2 filter).

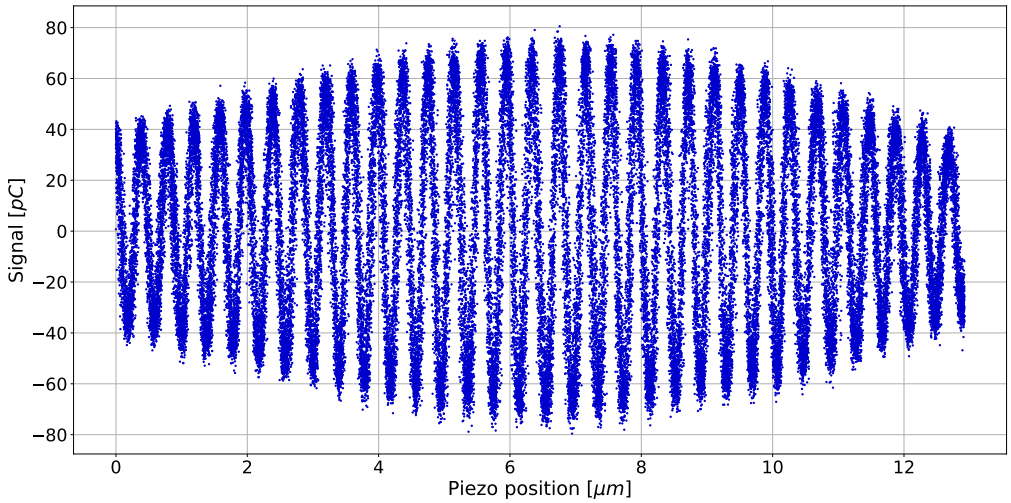

Figure 2.9: First order autocorrelation scan

We use the first order autocorrelation scan in order to find the region where the two pulses are completely overlapped. Once this region is found, we start scanning with the piezo stage. In the traces that will follow the scan was performed with 240 steps (i.e. 40 steps/cycle) and the piezo stayed at each step for 2 seconds, namely: $2\left[\frac{sec}{step}\right] \times 500\left[\frac{points}{sec}\right] = 10^3\left[\frac{points}{step}\right]$ (the sample rate is 500 Hz) . The first scan was done keeping the same power ratio between the LO and the signal.

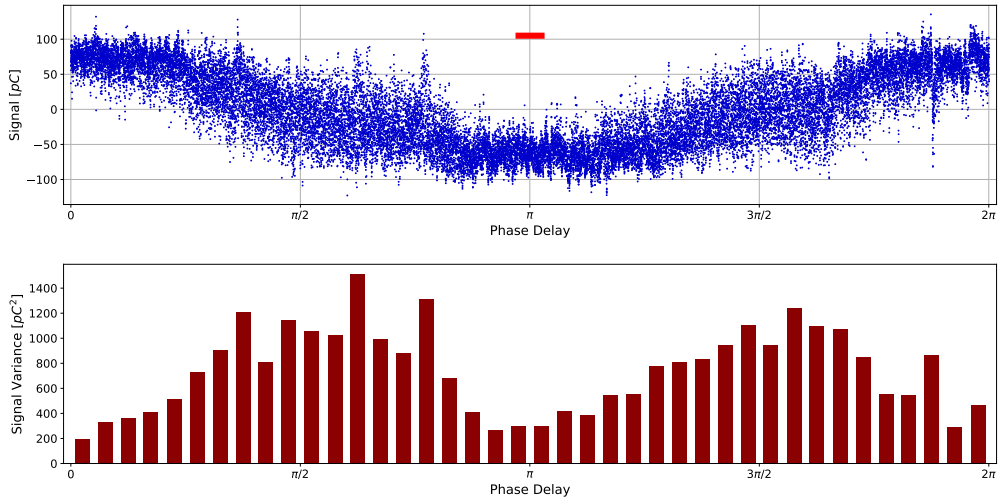

Figure 2.10: Homodyne trace with $P_{signal}/P_{LO} \approx 10^{-2}$. The upper figure, is the homodyne signal with respect to phase difference between the LO and the signal. The figure below is the variance calculated for each step−window (red bar in the upper panel of the figure).

Comparing the figure above with Fig.1.2, it is obvious that we cannot measure the coherent state of light under these conditions. The classical noise coming from the interferometer itself is much higher than the quantum noise. The effect of the classical noise is more apparent between the extrema of the laser cycle because the slope is higher and therefore small phase changes (due to the classical noise) have greater impact on the quadrature value. The Fourier transform of the signal will give us an insight into the frequencies that compose the given signal.

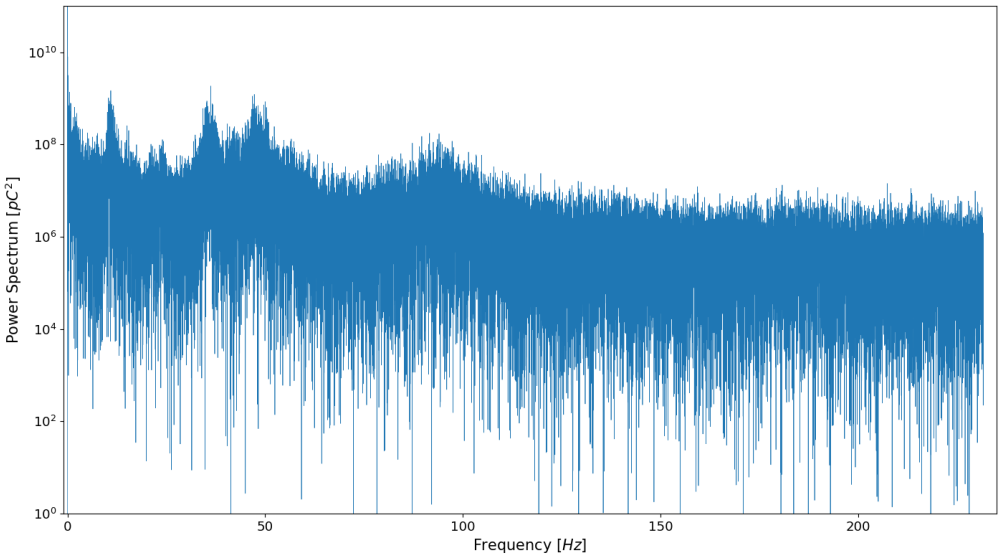

Figure 2.11: Power spectrum of the homodyne signal shown in fig. 2.10. The frequency axis of this graph has the units of inverse time because the Fourier transform was performed originally to the signal as a function of the time−stamp of each measurement point.

The quantum noise can be characterized as white noise. That means that is extended in all the spectrum and its amplitude in a power spectrum graph is almost constant for all the frequencies. The figure 2.11 indicates that this in not our case. In order to rid the homodyne signal of these external noise sources we perform a *Band Block* filter to the frequencies $0 - 170$ Hz. More specifically, notice that there is a quite broad peak at $\sim$100 Hz and a less conspicuous broad peak at $\sim$130 Hz. To be safe, we extended the band of the blocked frequencies up to 170 Hz, where the power spectrum seems to be flat, since no peak structure is observed thereafter. We note that this frequency is in agreement with the frequency obtained by the 1/(stability time) of Allan deviation when a small time interval around the $\pi/2$ value of the trace (where the amplitude is considers stable) was used. The exact procedure we followed is: a) we fit a sinusoidal function to the homodyne signal, b) we perform the band block filter, c) we add the inverse Fourier transform to the fitted sinusoidal function.

The application of the procedure mentioned above, to the signal of fig.2.10 has some interesting points worth noticing (fig. 2.12). First of all, it is obvious that most of the

classical noise has been removed by the *band block filter* since the average variance of the signal (we do not take into account the sinusoidal modulation) has dropped of about $1-2$ orders of magnitude. However, a ~ 200 % enchantment of signal variance around $\pi/2$ is still observed, which means that the amplitude of classical noise at frequencies ≥ 170 Hz is greater than the quantum noise. According to 1.73 in order to fix this problem we need to further reduce the amplitude of the signal field. In this way the amplitude of the classical noise can be significant smaller compared to the amplitude of the quantum noise which is independent on the amplitude of the signal field.

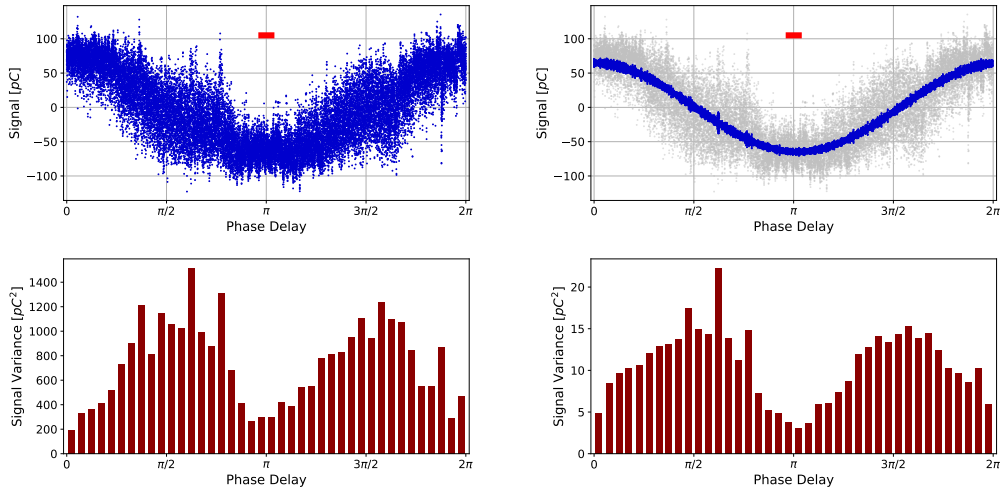

Figure 2.12: On the left we see the raw data obtained, while on the right there is the same signal after the frequency band block filter. The lower panels show the corresponding calculated variances.

Something else that we want to comment at this point is the detector's baseline drift that we mentioned earlier. A first estimate indicates that since we apply a block filter to the frequency band $0-170$ Hz, there is no need to search for a linear baseline drift because such kinds of drift are interpreted into low frequency peaks in the power spectrum. In order to confirm this estimation we applied the *overlapped Allan variance* algorithm to the homodyne signal of vacuum state input (i.e. blocked signal arm). The results are presented below fig. 2.13. The Figs.2.13a,2.13b we show the Allan variance (before and after recalibration) of the vacuum state as is presented in Fig. 2.6b. Fig. 2.13c shows the Allan variance (after recalibration) of the vacuum state for a recording time window corresponding to the time needed to record one cycle of the field. Fig. 2.13d shows the Allan variance (after recalibration) of the vacuum state after applying the band block filter in a recording time window of one cycle of the field. As we expected, the baseline linear drift has been removed since the Allan variance continuously drops. Also, the minimum Allan variance value is about two orders of magnitude lower because the band block filter removed most of the signal noise, as well.

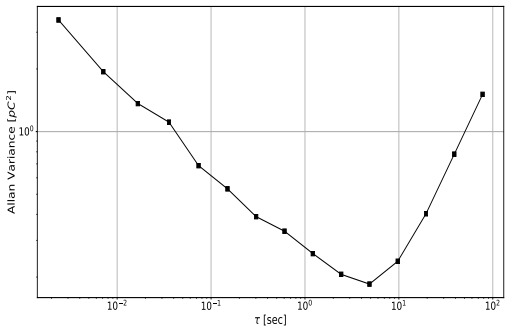

(a) Original full scan

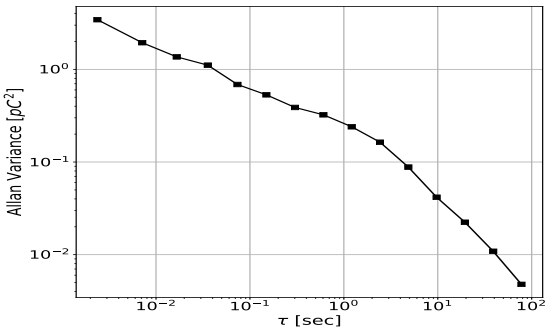

(b) Full scan after recalibration

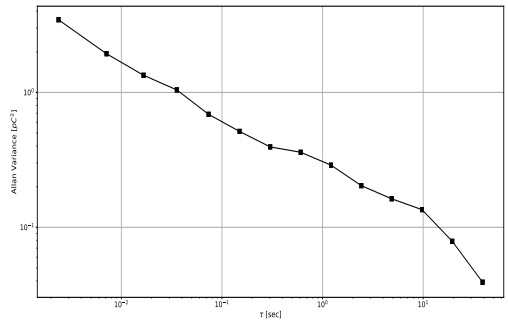

(c) One cycle range after recalibration

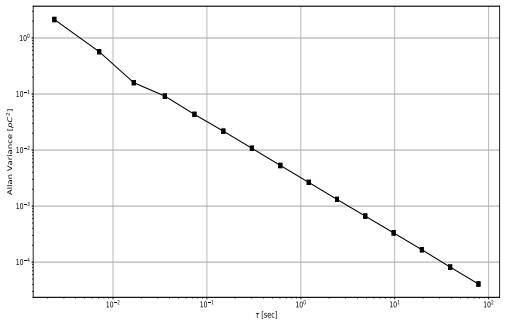

(d) After *band block* filter

Figure 2.13: Overlapped Allan variance calculation for a) the raw data signal b) the recalibrated signal c) one cycle temporal window after reclaibration and d) the signal after applying the frequency band block filter

2.7 Quadrature Measurements

2.7.1 Introduction

In this section we will present in detail the procedure used to analyze the homodyne traces. In section 1.5, it is shown that the homodyne signal is proportional to the generalized quadrature operator, $\hat{x}_\Phi$, where Φ is the relative phase between the LO and the signal field input. The analysis presented in this section contains a rescaling procedure, so that each point in the homodyne trace represent a measurement of the signal field quadrature. From the rescaled homodyne traces we can now calculate the mean photon number of the coherent state.

2.7.2 Vacuum state treatment

The vacuum input state was used as reference in order to calculate the rescaling factor. According to 1.74, the expectation value of the quadrature operator for vacuum state ($|0\rangle$) input signal is:

$$\langle \hat{x}_\Phi \rangle_{|0\rangle} = \frac{1}{2}\langle 0|(\hat{a}e^{-i\Phi} + \hat{a}^\dagger e^{i\Phi})|0\rangle = 0 \tag{2.2}$$

while the uncertainty is:

$$(\Delta\hat{x}_\Phi)^2_{|0\rangle} = \langle \hat{x}^2_\Phi \rangle_{|0\rangle} = \frac{1}{4}\langle 0|\hat{a}\hat{a}^\dagger + \hat{a}^\dagger\hat{a}|0\rangle = \frac{1}{4}\langle 0|1 + 2\hat{a}^\dagger\hat{a}|0\rangle = \frac{1}{4} \tag{2.3}$$

The uncertainty of a measured quantity "y" is given from the following formula:

$$\begin{aligned}(\Delta y)^2 &= \langle y^2\rangle - \langle y\rangle^2 \\ &= \frac{1}{N}\sum_{i=1}^{N}(y_i - \bar{y})^2 \\ &= \frac{1}{N}\sum_{i=1}^{N}\left(y_i - \frac{1}{N}\sum_{j=1}^{N} y_j\right)^2\end{aligned} \tag{2.4}$$

In order to rescale our signal, we want the factor λ which multiplies each measured point so as the variance of the quadrature operator for vacuum state input to become $\frac{1}{4}$. Therefore, in the eq. 2.4 we substitute $y_i \to \lambda y_i$ and we get:

$$\begin{aligned}(\Delta y)^2_{new} &= \frac{1}{N}\sum_{i=1}^{N}\left(\lambda y_i - \frac{1}{N}\sum_{j=1}^{N}\lambda y_j\right)^2 \\ &= \lambda^2(\Delta y)^2_{old}\end{aligned} \tag{2.5}$$

Thus, the proportionality factor λ is:

$$\lambda = \sqrt{\frac{(\Delta y)^2_{new}}{(\Delta y)^2_{old}}} = \frac{1}{\sqrt{4 \times (\Delta y)^2_{old}}} \tag{2.6}$$

Now, after we apply the frequency band block to the measured homodyne trace for the vacuum state, we calculate its variance. Then, we calculate the factor λ from equation 2.6. In our case, the value of this factor is:

$$\lambda = 0.3259 \quad \left[\frac{1}{Cb}\right] \tag{2.7}$$

In the following figure we present the vacuum state homodyne signal after the frequency band block filter (gray points) and the rescaled signal after the multiplication with the proportionality factor λ we calculated before.

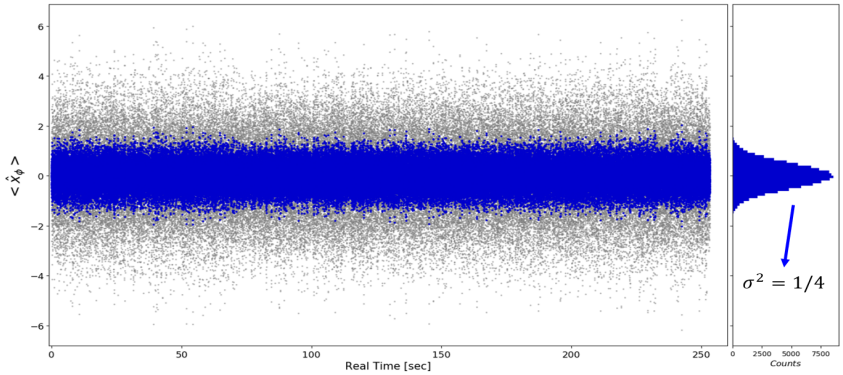

Figure 2.14: Homodyne trace for vacuum input state rescale so as the variance of the signal equals to 1/4

2.7.3 Coherent State homodyne traces

As we mentioned earlier, in order to measure correctly the coherent state of light, the classical noise needs to be less than the quantum noise. Therefore, we added two more OD filters (OD> 4) to the signal arm of the interferometer. In the graph below, we compare the Fourier transform of the coherent state input signal before and after the addition of these two OD filters. As we expected, the noise is significantly dropped

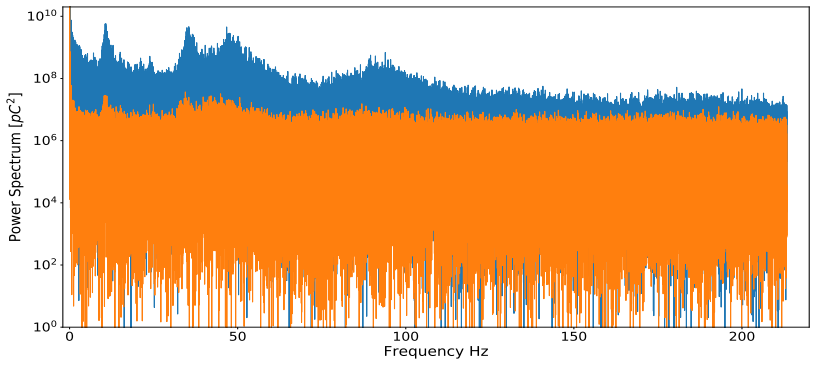

Figure 2.15: Fourier transform of the homodyne trace with coherent state input signal before (blue line) and after (orange line) the additional two OD filters. Significant noise reduction is observed.

with the additional attenuation of the signal arm. Most of the frequency peaks vanished, but we don't know if the classical noise is reduced enough. Following the same steps mentioned earlier, including the rescaling factor, we present the resulting traces for three different attenuations of the signal arm. On the left of figure 2.16 we present the final form of the homodyne traces, while on the right are the calculated variances.

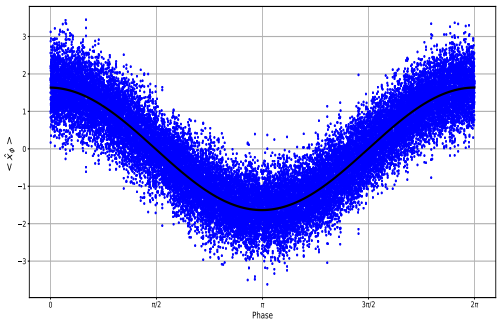

(a) $P_{signal}/P_{LO} \approx 10^{-5}$

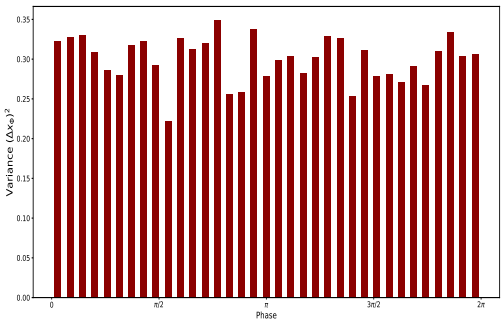

(b)

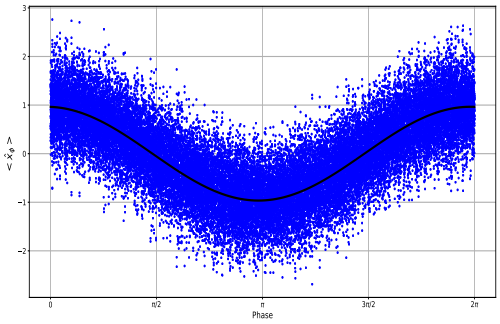

(c) $P_{signal}/P_{LO} \approx 10^{-6}$

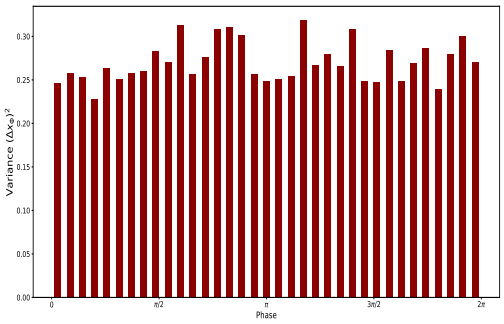

(d)

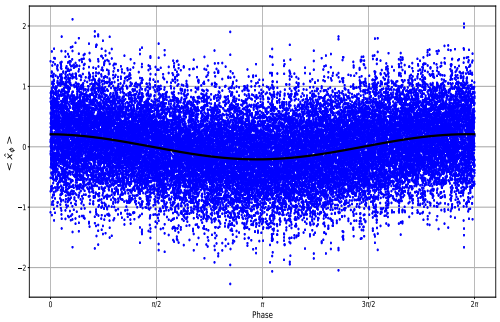

(e) $P_{signal}/P_{LO} \approx 10^{-7}$

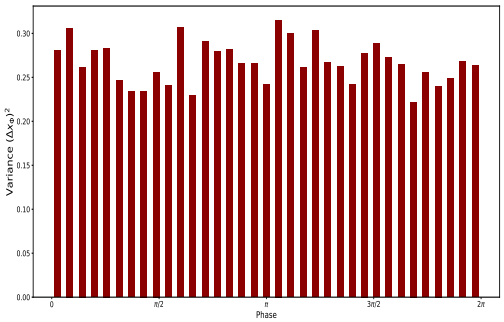

(f)

Figure 2.16: Homodyne traces after rescale. The optical density of the filter in the signal arm is approximately a) 4-5 c) 5-6 d) 6-7. In the figures b), d) and f) the respective variance calculation is depicted.

The mean photon number results from the expectation value of the quadrature operator since:

$$\langle \hat{x}_\Phi \rangle_{|\alpha\rangle} = |\alpha| cos(\Phi) \tag{2.8}$$

$$\langle \hat{n} \rangle = \langle \alpha | \hat{a}^\dagger \hat{a} | \alpha \rangle = |\alpha|^2 \tag{2.9}$$

where the eigenvalue α was written as $\alpha = |\alpha| e^{i\theta}$ and the phase θ is absorbed by phase Φ

in the expression above. Therefore, the amplitude of each cosine fitted function squared gives us the mean photon number of the coherent state input. In the table below we summarize the results of figure 2.16.

	$\langle\hat{n}\rangle$	$(\Delta\hat{x}_\Phi)^2 \pm \sigma$	Deviation (σ)
1	2.70	0.30 ± 0.03	1.67
2	0.93	0.27 ± 0.02	1
3	0.04	0.27 ± 0.02	1

Table 2.1: Summary of the experimental results

Few comments about the results presented in table 2.1. The calculation of the mean photon number results from the equations 2.8 and 2.9. The cosine fit function provides us the amplitude ($|\alpha|$) of eq.2.8, then is straight forward to calculate the mean photon number. The variance of the quadrature operator was calculated by taking the mean value of the variances presented in figure 2.16 for each homodyne trace. The error is the standard deviation of the variance calculations within a laser cycle. The last column of the table contains the deviation of the calculated uncertainty from the theoretical value 1/4. It is safe to say that in the homodyne traces we presented, we managed to measure the coherent state signal since the uncertainty values deviate from the theoretical value less than 3 standard deviations. Furthermore, the variance do not appear a specific structure like that of figure 2.10. There is no preferential phase region where the individual variances exceed the theoretical value, or the opposite. However, in the first homodyne trace, where the optical density of the filters in the signal arm was less, the deviation of the uncertainty value is bigger. Thus, we conclude that even in this case, the attenuation was not sufficient to suppress the classical noise much beyond the quantum noise. Nevertheless, the classical noise constitutes a quite small fraction, since no specific structure is apparent.

Last but not least, in perfect/ideal experimental conditions where no other noise is present to the homodyne trace except from the quantum noise, it wouldn't be necessary to perform any frequency band block filter. In the power spectrum, the only frequency peak would be the one which corresponds to the carrier frequency ω_c. The rest would be white noise. Unfortunately, this is not our case. Due to the influence of the classical noise, we are "forced" to apply such kind of frequency filter.

Conclusions

To summarize, we developed an experimental setup for the measurement of the quantum state of light, which is based on Mach-Zehnder interferometer and the utilization of an amplified balanced homodyne detector. After the complete characterization of the detection system and the stability of the interferometer we concluded that the quantum state of light can be measured if the ratio between the *Local Oscillator* and the *Signal Field* is $P_{LO}/P_{Signal} > 10^6$. This was achieved by measuring the coherent state of light produced by a Ti:Sapphire pulsed LASER source whose pulses duration is ≈ 40 fs.

Appendix

Our aim is to prove that the phase space graph of the coherent state 1.4 is a uniform Gaussian distribution. As it is presented in the main text, the quantization of the E/M field leads to the following expression of the annihilation ($\hat{a}$) and creation ($\hat{a}^\dagger$) operators:

$$\begin{aligned} \hat{a} &= (2\hbar\omega)^{-1/2}(\omega\hat{q} + i\hat{p}) \\ \hat{a}^\dagger &= (2\hbar\omega)^{-1/2}(\omega\hat{q} - i\hat{p}) \end{aligned} \tag{2.10}$$

The *Quadrature Operators* are correspondingly expressed as:

$$\begin{aligned} \hat{X} &= \left(\frac{\omega}{2\hbar}\right)^{1/2}\hat{q} \\ \hat{Y} &= \frac{1}{\sqrt{2\hbar\omega}}\,\hat{p} \end{aligned} \tag{2.11}$$

Since the quadrature operators are proportional to the operators $\hat{q}$ and $\hat{p}$, $|q\rangle$ and $|p\rangle$ are also eigenstates of the quadrature operators, with eigenvalues $(\omega/2\hbar)^{1/2}\,q$ and $1/\sqrt{2\hbar\omega}\;p$, respectively. We will now change the base we are working for reasons which will be obvious in the result.
Our new eigenstates are,

$$\begin{aligned} \left|\left(\frac{\omega}{2\hbar}\right)^{1/2} q\right\rangle &= |x\rangle, \quad (\hat{X}) \\ \left|\frac{1}{\sqrt{2\hbar\omega}}\;p\right\rangle &= |y\rangle, \quad (\hat{Y}) \end{aligned} \tag{2.12}$$

which are proportional to $|q\rangle$ and $|p\rangle$, respectively.

$$\begin{aligned} |q\rangle &= b|x\rangle \\ |p\rangle &= c|y\rangle \end{aligned}$$

Therefore, for the normalization of the $|x\rangle$ eigenstates we get:

$$\langle x'|x\rangle = \delta(x'-x) \Rightarrow b^{-2}\langle q'|q\rangle = \delta\Big[\left(\frac{\omega}{2\hbar}\right)^{1/2}(q'-q)\Big] \Rightarrow$$

$$b^{-2}\langle q'|q\rangle = \left(\frac{2\hbar}{\omega}\right)^{1/2}\delta(q'-q) \Rightarrow b = \left(\frac{\omega}{2\hbar}\right)^{1/4} \tag{2.13}$$

Similarly,

$$c = \left(\frac{1}{2\hbar\omega}\right)^{1/4} \tag{2.14}$$

Now we need to express the *coherent state* $|\alpha\rangle$ in terms of these eigenstates ($|x\rangle, |y\rangle$)

$$|\alpha\rangle = \hat{1}|\alpha\rangle = \int_{-\infty}^{\infty} dx \ \langle x|\alpha\rangle |x\rangle \tag{2.15}$$

we have also expressed coherent state as: $|\alpha\rangle = D(\alpha)|0\rangle$

$$|\alpha\rangle = D(\alpha)|0\rangle, \quad D(\alpha) = e^{\alpha\hat{a}^\dagger - \alpha^*\hat{a}} \tag{2.16}$$

The next step is to write the exponential supercript in terms of the operators $\hat{q}$ and $\hat{p}$. Therefore, using the Eq.2.10 and $\alpha = |\alpha|e^{i\theta}$:

$$\alpha\hat{a}^\dagger - \alpha^*\hat{a} = i|\alpha|\sqrt{\frac{2\omega}{\hbar}}\sin(\theta)\hat{q} - i|\alpha|\sqrt{\frac{2}{\hbar\omega}}\cos(\theta)\hat{p} \tag{2.17}$$

If we consider as $\hat{A}$ the first term and $\hat{B}$ the second term of Eq.2.17, then we get the following commutation relation:

$$[\hat{A}, \hat{B}] = i|\alpha|^2\sin(2\theta) = constant \tag{2.18}$$

thus, we can use the *Baker-Campell-Haussdorf* relation Eq.1.38 and end up to the following expression for the coherent state:

$$|\alpha\rangle = e^{-i\frac{|\alpha|^2}{2}\sin(2\theta)}e^{i|\alpha|\sqrt{\frac{2\omega}{\hbar}}\sin(\theta)\hat{q}}e^{-i|\alpha|\sqrt{\frac{2}{\hbar\omega}}\cos(\theta)\hat{p}}|0\rangle \tag{2.19}$$

Now we take the inner product with the $\langle q|$ on both sides

$$\langle q|\alpha\rangle = e^{-i\frac{|\alpha|^2}{2}\sin(2\theta)}e^{i|\alpha|\sqrt{\frac{2\omega}{\hbar}}\sin(\theta)\ q}e^{-|\alpha|\sqrt{\frac{2\hbar}{\omega}}\cos(\theta)\frac{\partial}{\partial q}}\psi_0(q) \tag{2.20}$$

where, $\psi_0(q)$ is the harmonic oscillator wavefunction for $n = 0$

$$\psi_0(q) = \left(\frac{\omega}{\pi\hbar}\right)^{1/4} e^{-\frac{q^2}{2(\hbar/\omega)}} \tag{2.21}$$

Note:
The Taylor series expansion of a function $f(x+b)$ around $x_0 = a$

$$f(x+b) = \sum_n \frac{f^{(n)}(a)}{n!}(x - a + b)^n$$

Let now $x_0 = x$. Then,

$$f(x+b) = \sum_n \frac{b^n f^{(n)}(x)}{n!} = e^{b\partial_x}f(x) \tag{2.22}$$

Therefore Eq.2.20 becomes

$$\langle q|\alpha\rangle = e^{-i\frac{|\alpha|^2}{2}\sin(2\theta)}e^{i|\alpha|\sqrt{\frac{2\omega}{\hbar}}\sin(\theta)\ q}\psi_0(q - q_0), \quad q_0 = |\alpha|\sqrt{\frac{2\hbar}{\omega}}\cos(\theta) \tag{2.23}$$

Using the eigenstates $|x\rangle$ which are related to eigenstates $|q\rangle$ according to the following equation

$$|q\rangle = \left(\frac{\omega}{2\hbar}\right)^{1/4} |x\rangle = \left(\frac{\omega}{2\hbar}\right)^{1/4} \left|\sqrt{\frac{\omega}{2\hbar}}\ q\right\rangle \tag{2.24}$$

we get:

$$\langle x|\alpha\rangle = \left(\frac{2}{\pi}\right)^{1/4} e^{-i\frac{|\alpha|^2}{2}\sin(2\theta)} e^{i2|\alpha|\sin(\theta)x} e^{-(x-|\alpha|\cos(\theta))^2} \tag{2.25}$$

Following similar steps for the $|p\rangle$ eigenstates we get:

$$\langle y|\alpha\rangle = \left(\frac{2}{\pi}\right)^{1/4} e^{-i\frac{|\alpha|^2}{2}\sin(2\theta)} e^{-i2|\alpha|\cos(\theta)y} e^{-(y-|\alpha|\sin(\theta))^2} \tag{2.26}$$

Finally, we have:

$$\begin{aligned} |\langle x|\alpha\rangle|^2 &= \left(\frac{2}{\pi}\right)^{1/2} e^{-\frac{(x-|\alpha|\cos(\theta))^2}{2(1/2)^2}} \\ |\langle y|\alpha\rangle|^2 &= \left(\frac{2}{\pi}\right)^{1/2} e^{-\frac{(y-|\alpha|\sin(\theta))^2}{2(1/2)^2}} \end{aligned} \tag{2.27}$$

In the above expressions it is apparent that coherent states can be considered as a superposition of either the $\hat{X}$ or $\hat{Y}$ operator. Both superpositions follow a Gaussian probability distribution with variance equal to $1/4$ and centered at $|\alpha|\cos(\theta)$ and $|\alpha|\sin(\theta)$ for $\hat{X}$ and $\hat{Y}$ operator, respectively. This result justifies the Coherent state plot in phase space, presented in the main text.

Acknowledgements

First of all, I would like to thank my supervisor not only for his guidance regarding the implementation of the experiment but also for his invaluable help in obtaining a deeper understanding of the nature of this experiment. I am also grateful for the patience of my colleagues Orfanos Ioannis and Makos Ioannis during late night experiments. Furthermore, I would like to thank my colleagues Liontos Ioannis and Skantzakis Manolis for their useful advice. Last but not least, I owe a big thank you to Papadakis Nikolaos who, helped me a lot with the construction of the Python scripts I used for the data analysis.

Bibliography

[1] Roy J. Glauber. Coherent and incoherent states of the radiation field. *Phys. Rev.*, 131:2766–2788, Sep 1963.

[2] Roy J. Glauber. Nobel lecture: One hundred years of light quanta. *Rev. Mod. Phys.*, 78:1267–1278, Nov 2006.

[3] C. Gerry and P. Knight. *Introductory Quantum Optics*. Cambridge University Press, 2004.

[4] R. Loudon. *The Quantum Theory of Light*. OUP Oxford, 2000.

[5] Gerd Breitenbach, Stephan Schiller, and J. Mlynek. Measurement of the quantum states of squeezed light. *Nature*, 387, 05 1997.

[6] A. I. Lvovsky and M. G. Raymer. Continuous-variable optical quantum-state tomography. *Rev. Mod. Phys.*, 81:299–332, Mar 2009.

[7] Shanna Du, Zongyang Li, Wenyuan Liu, Xuyang Wang, and Yongmin Li. High-speed time-domain balanced homodyne detector for nanosecond optical field applications. *J. Opt. Soc. Am. B*, 35(2):481–486, Feb 2018.

[8] D. W. Allan. Statistics of atomic frequency standards. *Proceedings of the IEEE*, 54(2):221–230, Feb 1966.